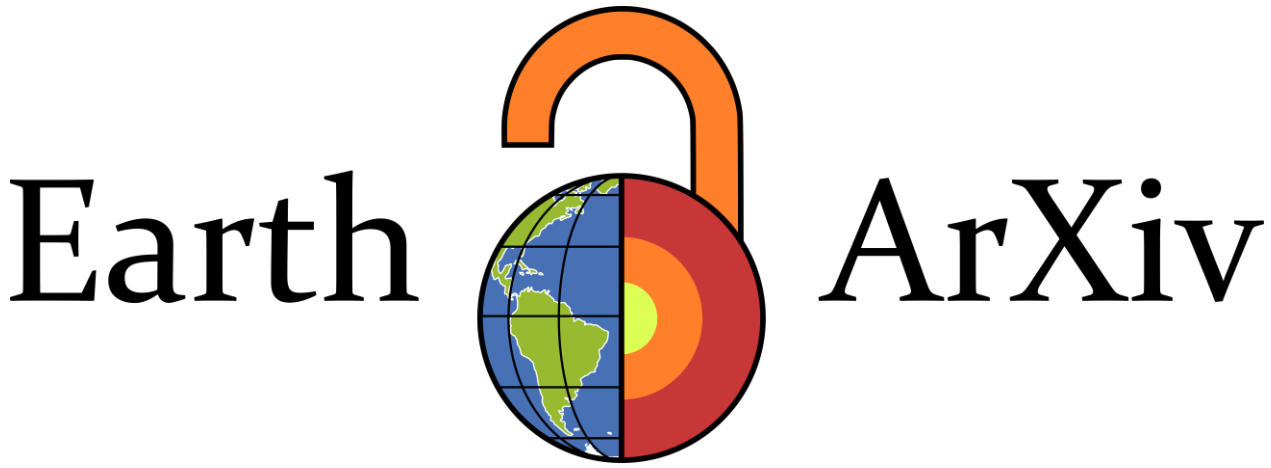


This is a non-peer-reviewed preprint submitted to EarthArXiv.

This manuscript has been submitted for publication in Landslides in the category Landslide News. Please note the manuscript has yet to be formally accepted for publication. Subsequent versions of this manuscript may have slightly different content. If accepted, the final version of this manuscript will be available via the ‘Peer-reviewed Publication DOI’ link on the right-hand side of this webpage. Please feel free to contact any of the authors; we welcome feedback.

Very-high-resolution optical imagery reveals key clues to the Langtang Lirung ice–rock avalanche

Tommaso Carlà [a,b*], *Veronica Tofani* [a,b], *Nicola Casagli* [a,b]

[a] *Department of Earth Sciences, Università degli Studi di Firenze, Via Giorgio La Pira 4, 50121 Florence, Italy*

[b] *UNESCO Chair on the Prevention and Sustainable Management of Geo-Hydrological Hazards, Università degli Studi di Firenze, Largo Enrico Fermi 2, 50125 Florence, Italy*

** corresponding author, e-mail address: tommaso.carla@unifi.it*

Abstract

Ice–rock avalanches and resulting cascading processes are increasingly recognized to pose an exceptional risk to high-mountain systems. Once initiated, they often transition from dense multiphase mixtures to water-saturated debris flows and even hyper-concentrated floods, thus attaining sufficient runout potential to move from highly remote to populated regions. The event that originated from the northern flank of the Langtang Lirung on 26 August 2026 is the most recent and dramatic example. Here we document an archive of 11 very-high-resolution (VHR) optical images of the avalanche source area, highlighting the overall stationarity of the glacier tongue in the 6 years preceding its collapse. In contrast, remarkable indicators of a deep-seated failure mechanism are observed in the outcropping bedrock, pointing to intrinsic rock mass structural weakness and long-term preconditioning as opposed to sudden climate-related triggering.

Introduction

Eyewitness videos and CCTV footage of the 26 August 2026 catastrophic flooding that struck the Nepal-Tibet border have widely circulated both on social media and in traditional news outlets due to the scale and sheer destructive power of the event. To date, more than a thousand fatalities have been confirmed—a number sadly destined to grow dramatically when taking into account that more than 5000 people remain missing, according to official reports. As the flooding was not attributable to unusual precipitation, attention promptly turned to the possibility of a cascading process chain of landslide- and/or glacier-related hazards. The frequency of these events is expected to increase across high-mountain systems worldwide affected by rapid glacier retreat and permafrost degradation (Zhong et al., 2024; Ahmed et al., 2026), as for example recently evidenced by the Chamoli (India), Marmolada (Italy), and Blatten (Switzerland) ice–rock avalanches (Shugar et al., 2021; Bondesan & Francese, 2023; Büntgen et al., 2025; Carlà et al., 2026).

A flurry of explanations regarding the source mechanism of the Nepal-Tibet flooding were thus theorized, including earthquake triggering, landslide damming, a glacier-lake outburst flood, a glacier collapse, or a combination thereof. However, seismic waves were later re-classified as consistent with a landslide or glacier collapse rather than an earthquake, and publicly available medium resolution optical imagery demonstrated that a valley lake was not present shortly before the disaster; additionally, only 7

minutes had passed between the onset of the seismic signal at Langtang Lirung and the arrival of the main debris flow surge at the Gyirong Port checkpoint, roughly 20 km downstream (Fig. 1a). Post-event imagery instead showed that a huge chunk of a glacial tongue had detached from the northern flank of the Langtang Lirung peak in Langtang National Park (Nepal), implying that most of the ice had consequently melted through frictional heating upon a vertical fall of more than 1 km (Petley, 2026). Part of an adjacent slope also appeared to have failed, possibly as a result of loss in lateral confinement after the glacier collapse.

This short contribution is the first to document very-high-resolution (VHR) optical imagery acquired before and after the Langtang Lirung ice–rock avalanche by the 30-, 42-, and 50-cm satellites of the Pléiades 1/Pléiades Neo (Airbus Defence and Space), GeoEye/WorldView/WorldView Legion (Vantor), and SuperView/SuperView Neo (China Siwei) constellations. Featuring the highest pansharpened resolutions commercially available, these images reveal key clues to the source mechanism, preconditioning factors, and precursory signs of the event, from which broader implications for the assessment and management of such hazard cascades in high-mountain systems can be derived.

VHR optical imagery

We compiled an archive of 11 VHR optical images of the northern flank of Langtang Lirung ranging from 18 March 2020 to 27 August 2026 (i.e., the day after the event). Table 1 summarizes the main acquisition details in terms of the angles of satellite azimuth (α_{sat}) and off-nadir (β_{sat}) as well as sun azimuth (α_{sun}) and elevation (β_{sun}). Unless specifically tasked over an area of interest, the considered satellite constellations offer highly variable revisit rates; hence, a selection could not be made by following a regular temporal pattern. Several candidate scenes were also discarded because they were associated with extensive cloud cover, high off-nadir angles, or low sun elevation. The products forming the compiled archive are arranged chronologically in Figs. 1b–f and 2a–f; critically, those dated 11 September 2024 and 27 August 2026 yield a snow-free overview of the slopes surrounding the glacier tongue.

Glacier behavior and evidences of slope instability

A first notable insight gained from a visual comparison of the images (e.g., Fig. 1d versus Fig. 2e) is that the glacier does not appear to have exhibited an appreciable retreat in the six years preceding its collapse. Although some geometrical distortions are introduced between images by the differing satellite azimuth and off-nadir angles at each acquisition, it can also be observed that the amount and distribution of the main crevasses did not change significantly over the same period, both in the area that eventually failed and upslope of it (e.g., Fig. 2b versus Fig. 2e). Enhanced crevassing could have otherwise been interpreted as an indicator of increasing basal sliding leading up to collapse (Kääb et al., 2018). This suggests that glacier instability did not play a primary role in the development of the Langtang Lirung ice–rock avalanche.

On the other hand, the aforementioned images characterized by reduced snow cover strongly support the proposition that the event was triggered by instability and collapse of the bedrock south of and underneath the glacier tongue (see zoomed-in details in Fig. 3). Major structural lineaments were in fact already visible in the 11 September 2024 acquisition, where the current U-shaped scarp formed (see Figs. 3a–c versus Fig. 3d). In particular, these include: a deep incision corresponding to the right lateral scarp (which is better captured by other images in the dataset, see Figs. 1–2); large cracking along much of the left lateral scarp (with sub-parallel and cross-cutting features located closely upslope, potentially denoting a tendency for further retrogression); and a trench-like depression tracing the portion of the head scarp not buried by the glacier tongue before the landslide (see three-dimensional view in Fig. 3c). In the same acquisition, the area downslope of the head and left lateral scarps also shows a marked change in color and surface texture with respect to nearby areas not involved in the collapse, possibly reflecting high rockfall activity. All the above point to the Langtang Lirung ice–rock avalanche as solely originating from the long-term evolution of a deep-seated rock slope failure mechanism, whereby the overlying glacier tongue was merely carried away once the sliding mass abruptly detached. Given that an accurate estimate of the source volume cannot be made without appropriate topographical information, it is worth emphasizing that the head scarp and lateral scarps each measure ~1 km, resulting in a source area of ~1 km^2. It follows that, as a first general approximation based on the empirical relationship by Guzzetti et al. (2009) and associated uncertainty, the source volume may reasonably range from 10^7 m^3 to more than 10^8 m^3, excluding the overlying ice mass.

Discussion and conclusions

Despite being relatively rare, cascading landslide and glacier hazards have recently been the subject of growing interest in light of their extraordinary mobility and geomorphic impact on increasingly populated high-mountain systems (Sosio, 2015; Zhong et al., 2025; Ahmed et al., 2026). Moreover, while a direct link has only been postulated and is yet to be proven, questions arise as to whether ongoing changes in climate, ice, and permafrost conditions may exacerbate their occurrence and effects (Huggel, 2009; Shugar et al., 2021; Zhong et al., 2024). The 26 August 2026 Langtang Lirung ice–rock avalanche is, in all likelihood, the most consequential event of this type in the last few decades. Preliminary findings from an archive of 11 VHR optical images allowed us to better circumstantiate its nature. We inferred that: i) the extent and crevasse pattern of the collapsed glacier tongue were broadly stationary in the preceding six years; ii) adjacent slopes were instead affected by distinct signs of rock mass damage and long-term instability; and iii) similar structures define a wedge-shaped sector bordered by another glacier tongue behind the current left lateral scarp (Fig. 3d), thus potentially posing a risk of a new ice–rock avalanche on a smaller scale.

The acquired images indicate that escalating glacial debuttressing, thermal disturbance, and permafrost degradation are unlikely to have acted as a sudden trigger of the collapse; rather, long-term trends of these processes may have preconditioned the slope for instability, which appears to have been mainly induced by intrinsic rock mass structure, oversteepening, and progressive failure mechanisms under sub-critical stress conditions (Eberhardt et al., 2004; Eberhardt, 2008; Brideau et al., 2009; Riva et al., 2018).

Another important implication is that, as evidenced by the 2021 Chamoli disaster (Shugar et al., 2021), extremely large runout distance and velocity can be attained even when the ice–rock mixture in the source volume is dominated by the latter of the two components. Future work should be aimed at reproducing the observed flow dynamics through multi-phase numerical modelling that accounts for frictional heating, thermal exchange effects, phase/regime transitions, and path entrainment (Munch et al., 2024; Zhuang et al., 2025; Singh et al., 2026). In this regard, no lake occupied the nearby valley floor at least up until 17 June 2026 (Fig. 2e), meaning that a contribution from prior landslide damming to the extraordinary mobility of the 26 August 2026 Langtang Lirung event cannot be invoked at present.

Enhanced orthorectification and co-registration of pre-event VHR images by exploiting high-resolution topographic information may also allow surface velocity estimates of the collapsed glacier tongue through offset tracking techniques, in search of a proxy for the impending detachment of the underlying sliding mass; however, deformation in rock slopes is typically much more subtle than that experienced by flowing alpine ice (Kääb, 2005; Liu et al., 2019; Troilo et al., 2024). The fact that the underlying mechanism at Langtang Lirung was a rock slope failure further underscores the challenges related to hazard assessment of ice–rock avalanches, as the evolution of large rock slope instabilities is known to be highly elusive—they may move either continuously or intermittently for a seemingly indefinite time, promote only episodic rockfall from the detachment of comparatively small sectors, eventually become inactive, or conversely evolve to catastrophic collapse (Crosta et al., 2017; Agliardi et al., 2020; Carlà et al., 2024). Early reports attest that no obvious precursor was detected by radar-based medium-resolution measurements from the Sentinel-1 constellation (Sah, 2026). This again calls for systematic monitoring of high-mountain systems through in situ campaigns and the combined exploitation of both radar and optical VHR satellite imagery.

Acknowledgements The authors are grateful to Brock Adam McCarty from Apollo Mapping for his kind and swift assistance in providing the VHR imagery.

Data availability The data supporting the findings of this study are available from the corresponding author upon reasonable request.

Statements and declarations *Competing interests.* The authors have no competing interests to declare.

Figure and table captions

Table 1 Main acquisition details of the acquired VHR optical images

Fig. 1 a Terrain map of the area surrounding the Langtang Lirung peak and acquired VHR imagery from **b** 18 March 2020, **c** 22 October 2021, **d** 16 October 2022, **e** 25 October 2023, and **f** 11 September 2024

Fig. 2 Acquired VHR imagery from **a** 25 October 2025, **b** 10 November 2025, **c** 2 January 2026, **d** 6 January 2026, **e** 17 June 2026, and **f** 27 August 2026

Fig. 3 Zoomed-in details of the outcropping bedrock south of the collapsed glacier tongue as seen on **a–c** 11 September 2024 and **d** 27 August 2026 (satellite imagery in **c** is draped onto Esri's basemap elevation layer)

References

Agliardi F, Scuderi MM, Fusi N, Collettini C (2020) Slow-to-fast transition of giant creeping rockslides modulated by undrained loading in basal shear zones. Nat Commun 11:1352. https://doi.org/10.1038/s41467-020-15093-3

Ahmed R, Bhardwaj A, Sam L, Van Tricht L (2026) Ice-rock avalanches in a warming Himalaya indicate pathways toward effective preparedness. Commun Earth Eviron 7:217. https://doi.org/10.1038/s43247-026-03352-y

Bondesan A, Francese RG (2023) The climate-driven disaster of the Marmolada Glacier (Italy). Geomorphology 431:108687. https://doi.org/10.1016/j.geomorph.2023.108687

Brideau M-A, Yan M, Stead D (2009) The role of tectonic damage and brittle rock fracture in the development of large rock slope failures. Geomorphology 103:30–49. https://doi.org/10.1016/j.geomorph.2008.04.010

Büntgen U, Oppenheimer C, Farinotti D, Nahtz T, Esper J (2025) The 2025 Blatten disaster in the Swiss Alps followed exceptional warming and highlights the vulnerability of people and heritage in glaciated landscapes. Commun Earth Eviron 6:994. https://doi.org/10.1038/s43247-025-02994-8

Carlà T, Gigli G, Lombardi L, Nocentini M, Gracchi T, Rossi G, Tacconi Stefanelli C, Raspini F, Fubelli G, Casagli N (2024) Mechanisms of block instability at the toe of a slowly deforming rock slope. Rock Mech Rock Eng 57:1543–1563. https://doi.org/10.1007/s00603-023-03674-9

Crosta GB, Agliardi F, Rivolta C, Alberti S, Dei Cas L (2017) Long-term evolution and early warning strategies for complex rockslides by real-time monitoring. Landslides 14:1615–1632. https://doi.org/10.1007/s10346-017-0817-8

Eberhardt E, Stead D, Coggan JS (2004) Numerical analysis of initiation and progressive failure in natural rock slopes—the 1991 Randa rockslide. Int J Rock Mech Min Sci 41:69–87. https://doi.org/10.1016/S1365-1609(03)00076-5

Eberhardt E (2008) Twenty-ninth Canadian Geotechnical Colloquium: The role of advanced numerical methods and geotechnical field measurements in understanding complex deep-seated rock slope failure mechanisms. Can Geotech J 45:484–510. https://doi.org/10.1139/T07-116

Gusmeroli A, Carlà T, Leva D, Rivolta C, Villa F, Casagli N (2026) Post-collapse ice cliff backwasting at the Marmolada Glacier observed by terrestrial radar interferometry. J Geophys Res Earth Surf 131: e2025JF008367. https://doi.org/10.1029/2025JF008367

Guzzetti F, Ardizzone F, Cardinale M, Rossi M, Valigi D (2009) Landslide volumes and landslide mobilization rates in Umbria, central Italy. Earth Planet Sci Lett 279:222–229. https://doi.org/10.1016/j.epsl.2009.01.005

Huggel C (2009) Recent extreme slope failures in glacial environments: effects of thermal perturbation. Quat Sci Rev 28(11–12):1119–1130. https://doi.org/10.1016/j.quascirev.2008.06.007

Kääb A (2005) Combination of SRTM3 and repeat ASTER data for deriving alpine glacier flow velocities in the Bhutan Himalaya. Remote Sens Environ 94(4):463–474

Kääb A, Leinss S, Gilbert A, Bühler Y, Gascoin S, Evans SG, Bartelt P, Berthier E, Brun F, Chao W-A, Farinotti D, Gimbert F, Guo W, Huggel C, Kargel JS, Leonard GJ, Tian L, Treichler D, Yao T (2018) Massive collapse of two glaciers in western Tibet in 2016 after surge-like instability. Nat Geosci 11:114–120. https://doi.org/10.1038/s41561-017-0039-7

Liu L, Jiang L, Sun Y, Wang H, Sun Y, Xu H (2019) Diurnal fluctuations of glacier surface velocity observed with terrestrial radar interferometry at Laohugou No. 12 Glacier, western Qilian mountains, China. J Glaciol 65(250):239–248. https://doi.org/10.1017/jog.2019.1

Munch J, Zhuang Y, Dash RK, Bartelt P (2024) Dynamic thermomechanical modeling of rock-ice avalanches: Understanding flow transitions, water dynamics, and uncertainties. J Geophys Res Earth Surf 129:e2024JF007805. https://doi.org/10.1029/2024JF007805

Petley D (2026) The 26 August 2026 catastrophic debris flow in Nepal and Tibet. https://eos.org/thelandslideblog/26-august-2026-nepal-and-tibet

Riva F, Agliardi F, Amitrano D, Crosta GB (2018) Damage-based time-dependent modeling of paraglacial to postglacial progressive failure of large rock slopes. J Geophys Res Earth Surf 123(1):124–141. https://doi.org/10.1002/2017JF004423

Sah AK (2026) No detectable precursor in Sentinel-1 backscatter before the 26 August 2026 Langtang Lirung rock–ice avalanche, Nepal. Preprint, https://doi.org/10.31223/X59N5N

Shugar DH, Jacquemart M, Shean D, Bhushan S, Upadhyay K, Sattar A, Schwanghart W, McBride S, Van Wyk de Vries M, Mergili M, Emmer A, Deschamps-Berger C, McDonnell M, Bhambri R, Allen S, Berthier E, Carrivick JL, Clague JJ, Dokukin M, Dunning SA, Frey H, Gascoin S, Haritashya UK, Huggel C, Kääb A, Kargel JS, Kavanaugh JL, Lacroix P, Petley D, Rupper S, Azam MF, Cook SJ, Dimri AP, Eriksson M, Farinotti D, Fiddes J, Gnyawali KR, Harrison S, Jha M, Koppes M, Kumar A, Leinss S,

Majeed U, Mal S, Muhuri A, Noetzli J, Paul F, Rashid I, Sain K, Steiner J, Ugalde F, Watson CS, Westoby MJ (2021) A massive rock and ice avalanche caused the 2021 disaster at Chamoli, Indian Himalaya. Science 373:300–306

Singh J, Sepúlveda SA, Williams-Jones G (2026) Characterisation and multiphase flow modelling of a rock avalanche turned into a supraglacial debris flow: Insights from Mt Job, British Columbia, Canada. Earth Surf Process Landforms 51(5):e70308. https://doi.org/10.1002/esp.70308

Sosio R (2015) Rock–snow–ice avalanches. In: Davies T, Rosser N, Shroder JF (eds) Landslide hazards, risks, and disaster, 2nd edn. Elsevier, pp. 199–247. https://doi.org/10.1016/B978-0-12-818464-6.00007-X

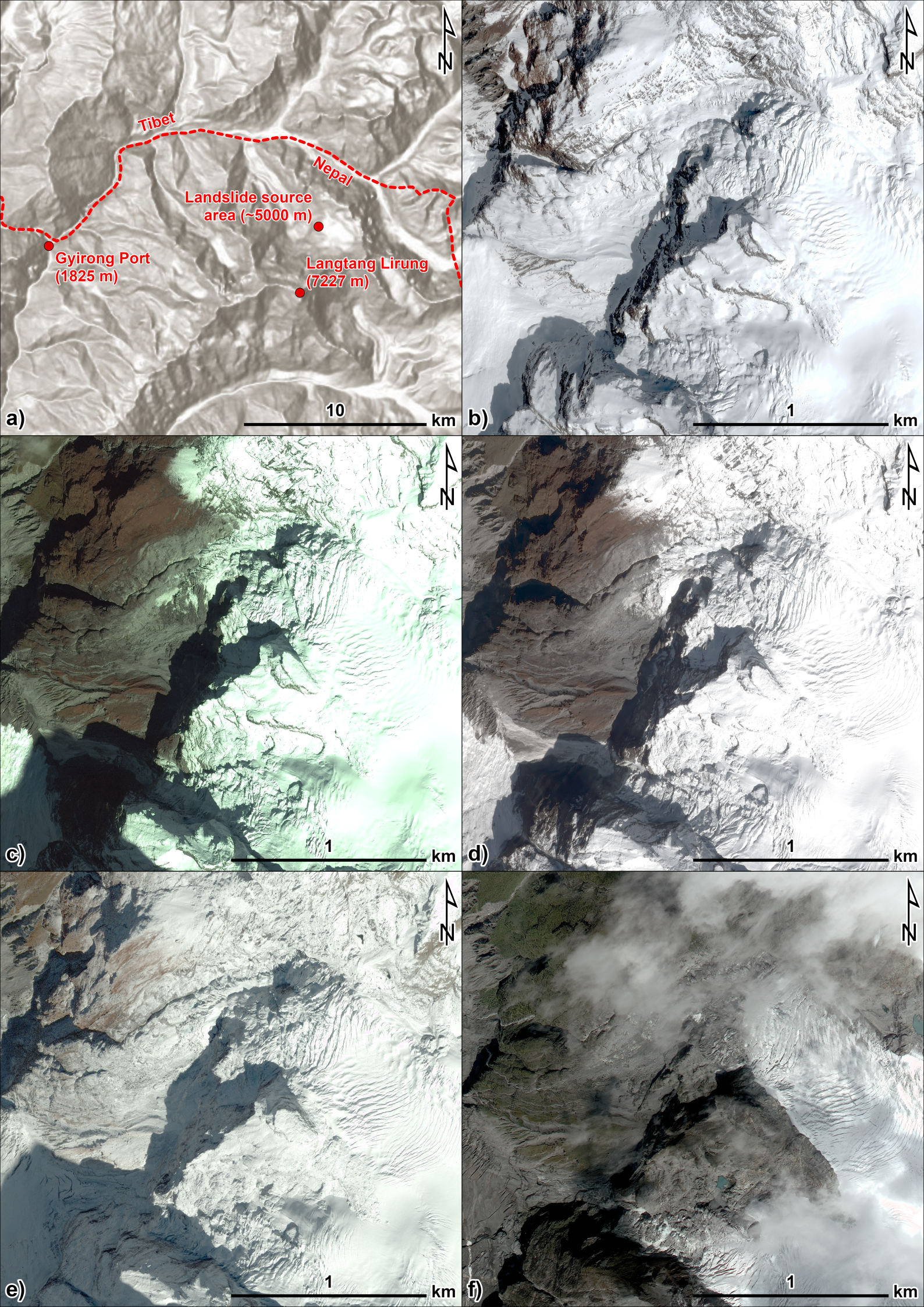
Troilo F, Dematteis N, Zucca F, Funk M, Giordan D (2024) Monthly velocity and seasonal variations of the Mont Blanc glaciers derived from Sentinel-2 between 2016 and 2024. Cryosphere 18:3891–3909. https://doi.org/10.5194/tc-18-3891-2024

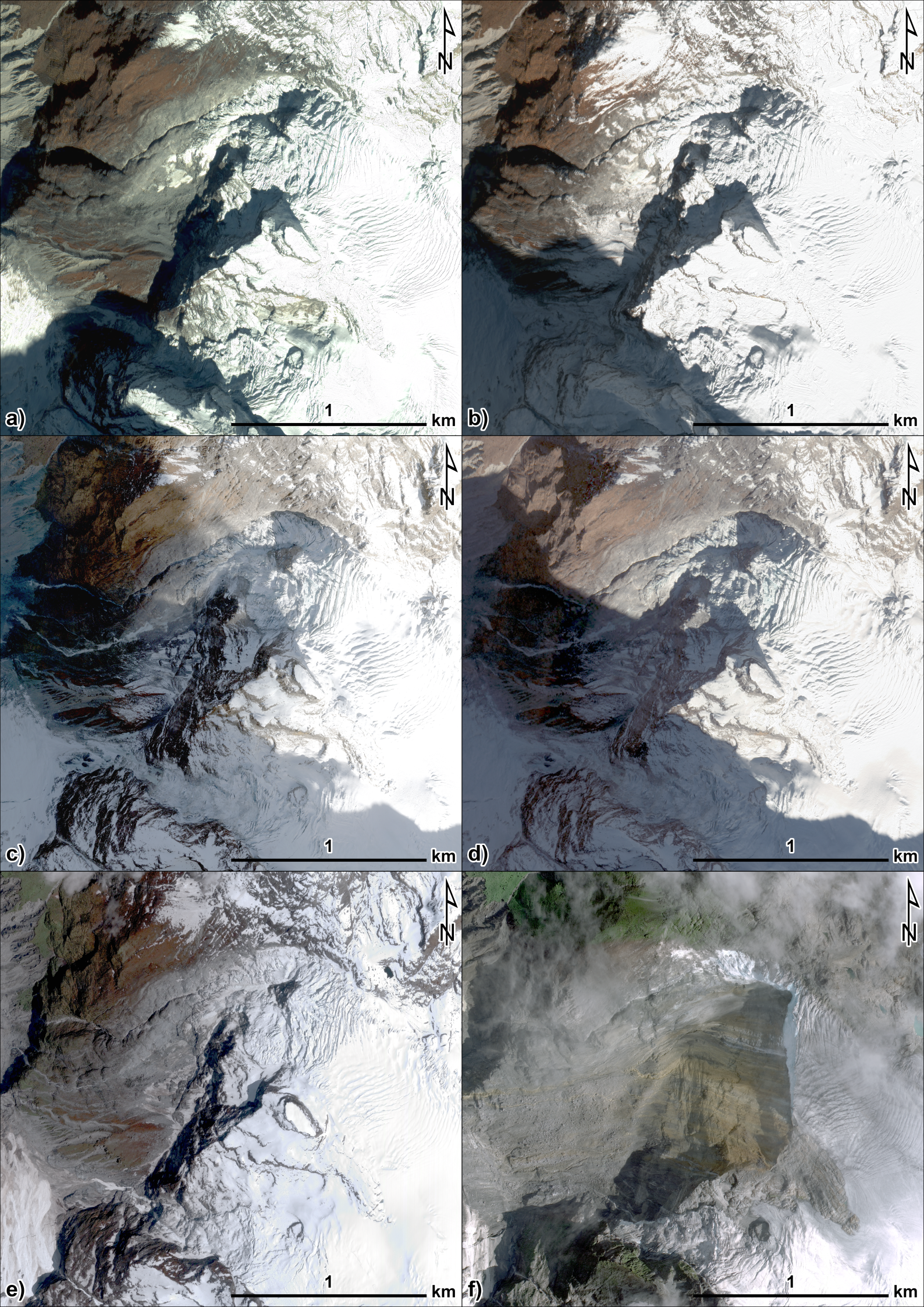
Zhong Y, Allen SK, Zheng G, Liu Q, Stoffel M (2024) Large rock and ice avalanches frequently produce cascading processes in High Mountain Asia. Geomorphology 449:109048. https://doi.org/10.1016/j.geomorph.2023.109048

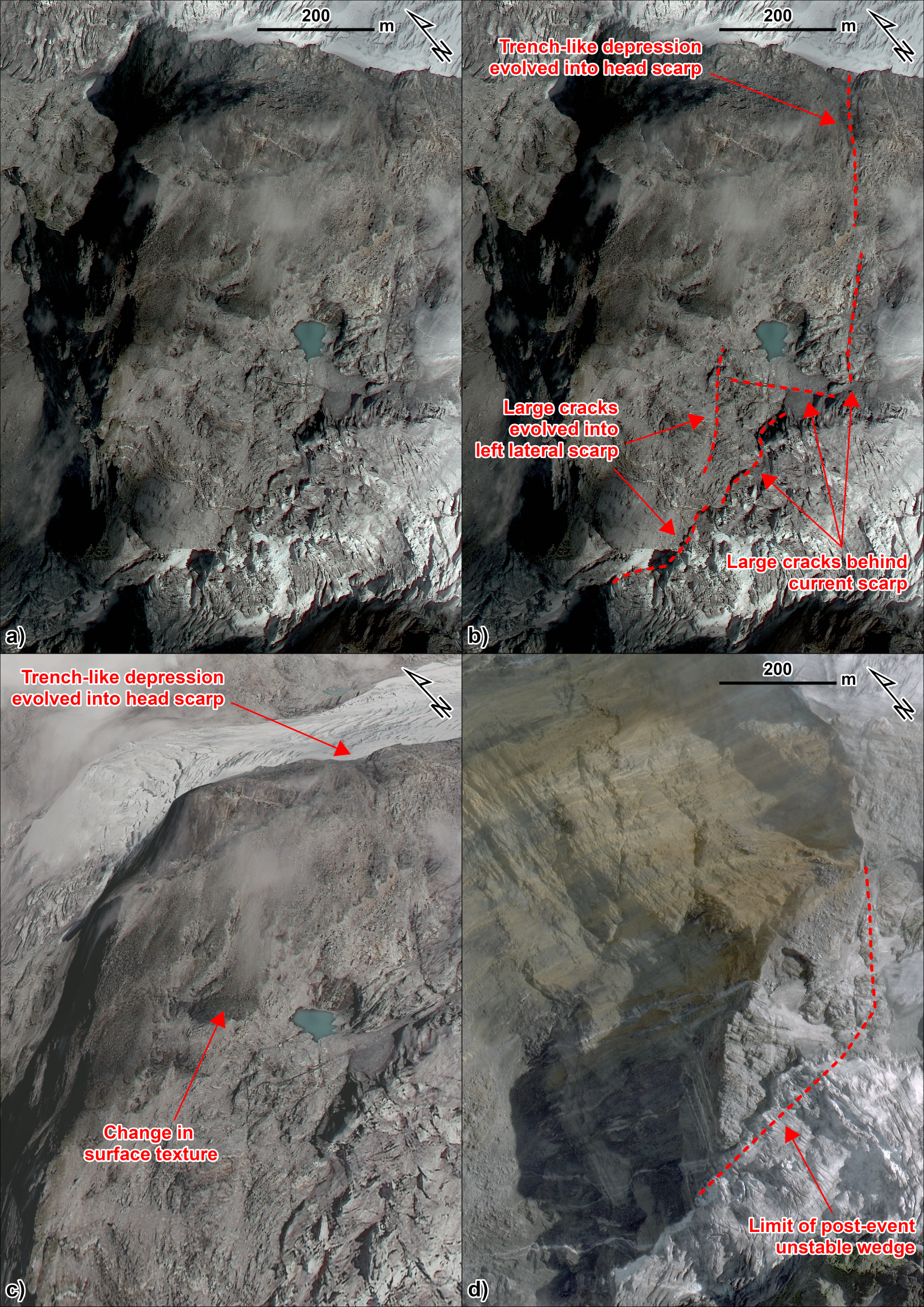
Zhong Y, Allen S, Li D, Corona C, Zheng G, Liu Q, Stoffel M (2025) Unravelling driving conditions of rock and ice avalanches and resulting cascading processes in High Mountain Asia. Landslides 22:989–1001. https://doi.org/10.1007/s10346-024-02421-7

Zhuang Y, Dash RK, Bühler Y, Chen R, Bartelt P (2025) Fluidization and snow cover effects in rock-ice-snow avalanches: Lessons from Piz Cengalo, Fluchthorn, and Piz Scerscen events. Comput Geotech 186:107456. https://doi.org/10.1016/j.compgeo.2025.107456

Date	Satellite	Resolution (cm)	α_{sat} (°)	β_{sat} (°)	α_{sun} (°)	β_{sun} (°)
18-Mar-2020	Pléiades 1	50	180	12.5	143.4	55.5
22-Oct-2021	WorldView-2	50	166.6	12.8	157.6	48.1
16-Oct-2022	Pléiades-1	50	180	18.2	159.2	51
25-Oct-2023	GeoEye-1	50	30.8	24.5	156.5	46.9
11-Sep-2024	SuperView-1	50	45.2	22.6	154	63.8
25-Oct-2025	SuperView Neo 3-02	50	61.3	3.3	161.9	47.7
10-Nov-2025	SuperView Neo 3-01	50	84.9	8.7	165.1	42.9
2-Jan-2026	Pléiades Neo 3	30	168.9	25.1	161	36.4
6-Jan-2026	SuperView Neo 3-01	50	72.5	0.3	161.8	36.8
17-Jun-2026	WorldView Legion 3	30	353.2	13.8	99.4	70.6
27-Aug-2026	SuperView-2	42	280.9	21.2	114.2	54.4


Tibet
Nepal
Landslide source area (~5000 m)
Gyirong Port (1825 m)
Langtang Lirung (7227 m)
a)
10
km
b)
1
km
c)
1
km
d)
1
km
e)
1
km
f)
1
km


a)
N
1
km
b)
N
1
km
c)
N
1
km
d)
N
1
km
e)
N
1
km
f)
N
1
km


200
m
N
a)
Trench-like depression
evolved into head scarp
Large cracks
evolved into
left lateral scarp
Large cracks behind
current scarp
b)
Trench-like depression
evolved into head scarp
Change in
surface texture
c)
d)
Limit of post-event
unstable wedge